# Spin-resolved photoelectron spectroscopy using femtosecond extreme ultraviolet light pulses from high-order harmonic generation

M. Plötzing, R. Adam', C. Weier, L. Plucinski, S. Eich, S. Emmerich, M. Rollinger, M. Aeschlimann, S. Mathias, and C. M. Schneider

Citation: Rev. Sci. Instrum. **87**, 043903 (2016); doi: 10.1063/1.4946782
View online: http://dx.doi.org/10.1063/1.4946782
View Table of Contents: http://aip.scitation.org/toc/rsi/87/4
Published by the American Institute of Physics

# Spin-resolved photoelectron spectroscopy using femtosecond extreme ultraviolet light pulses from high-order harmonic generation

M. Plötzing,[1] R. Adam,[1,a)] C. Weier,[1] L. Plucinski,[1] S. Eich,[2] S. Emmerich,[2] M. Rollinger,[2] M. Aeschlimann,[2] S. Mathias,[3] and C. M. Schneider[1]
[1]*Forschungszentrum Jülich GmbH, Peter Grünberg Institut (PGI-6), 52425 Jülich, Germany*
[2]*University of Kaiserslautern and Research Center OPTIMAS, 67663 Kaiserslautern, Germany*
[3]*Georg-August-Universität Göttingen, I. Physikalisches Institut, 37077 Göttingen, Germany*

(Received 12 October 2015; accepted 31 March 2016; published online 14 April 2016)

The fundamental mechanism responsible for optically induced magnetization dynamics in ferromagnetic thin films has been under intense debate since almost two decades. Currently, numerous competing theoretical models are in strong need for a decisive experimental confirmation such as monitoring the triggered changes in the spin-dependent band structure on ultrashort time scales. Our approach explores the possibility of observing femtosecond band structure dynamics by giving access to extended parts of the Brillouin zone in a simultaneously time-, energy- and spin-resolved photoemission experiment. For this purpose, our setup uses a state-of-the-art, highly efficient spin detector and ultrashort, extreme ultraviolet light pulses created by laser-based high-order harmonic generation. In this paper, we present the setup and first spin-resolved spectra obtained with our experiment within an acquisition time short enough to allow pump-probe studies. Further, we characterize the influence of the excitation with femtosecond extreme ultraviolet pulses by comparing the results with data acquired using a continuous wave light source with similar photon energy. In addition, changes in the spectra induced by vacuum space-charge effects due to both the extreme ultraviolet probe- and near-infrared pump-pulses are studied by analyzing the resulting spectral distortions. The combination of energy resolution and electron count rate achieved in our setup confirms its suitability for spin-resolved studies of the band structure on ultrashort time scales. *Published by AIP Publishing.* [http://dx.doi.org/10.1063/1.4946782]

## I. INTRODUCTION

Early experiments in the 1990s showed that the magnetization of thin magnetic films can be quenched on a subpicosecond time scale when the electron system is excited by an intense, ultrashort light pulse.[1] Since then, the topic has been extensively investigated both theoretically and experimentally. Theories based on phonon-mediated spin-flip scattering[2] and super-diffusive spin-currents[3] are at present showing the potential to explain the broad range of experimental results. However, the fundamental physical processes are still under strong debate. On the experimental side, the investigations have been dominated for a long time by photon-in/photon-out pump-probe measurements using femtosecond pulsed lasers.[2,4] Recently, the use of femtosecond bursts of high energy photons from free-electron lasers (FELs),[5] synchrotron femtoslicing,[6] and laser-based high-order harmonic generation (HHG)[7] in reflection, transmission, and absorption experiments has expanded remarkably our understanding of ultrafast magnetization dynamics by including element-selectivity.[8–11] Nevertheless, an even deeper understanding requires a close insight into basic material properties. Such a fundamental step is expected from mapping the time evolution of the ferromagnetic electronic band structure using spin-resolved photoelectron spectroscopy (PES). Up to now, most ultrafast time-resolved photoemission experiments addressing spin dynamics were limited by the low photon energies of pulsed lasers[12–14] allowing access only to electrons with low binding energies and limited wave vectors. The accessibility of the full Brillouin zone (BZ) and therefore the need for higher photon energies were additionally stressed by a study, which observed differences in the ultrafast response measured by the magneto-optic Kerr effect in the visible spectral range and by spin-resolved photoemission experiments.[15] Here, the authors suggest the sensitivity to different electronic states of both techniques as an explanation for this disagreement.

During recent years, it has been demonstrated that FELs can be employed for femtosecond time-resolved PES measurements.[16] At the same time, HHG sources showed their strong potential for expanding our knowledge by mapping the fastest dynamics of the electronic band structure in energy-, time-, and angle-resolved experiments.[17–21] In order to disentangle the processes involved in the angular momentum dissipation in ultrafast demagnetization, it is necessary to add spin-sensitivity to the detection of photoelectrons. It has been demonstrated earlier that the combination of a Mott spin detector and FEL radiation can be used for studies of laser-induced changes in the total magnetization of Fe by measuring the spin polarization of the secondary electrons.[22] However, the low repetition rates of available FELs in the Hz range and the limitation of the maximum pulse intensity due to Coulomb repulsion in the resulting dense electron clouds (see Sec. IV)

a)Electronic mail: r.adam@fz-juelich.de

restrict the number of photoelectrons in such experiments. Due to the latter, as well as due to the low efficiency of previous spin detection techniques, combined energy- and spin-resolved experiments with a sub-picosecond temporal resolution and photon energies by far exceeding the visible range have, to our knowledge, not been performed up to now.

Here, we present a new approach that connects a HHG-based extreme ultraviolet (XUV) light source with a state-of-the-art spin detector. Our femtosecond-pulsed XUV source provides *two orders of magnitude higher repetition rates* compared to current FELs and the spin detection is *a factor of 20 more efficient* than in Mott- or spin polarized low energy electron diffraction (SPLEED)-based (single-channel) detectors.[23] The presented spectra demonstrate for the first time the feasibility of spin-resolved PES with a HHG light source. Furthermore, our analysis shows the strong potential of our approach for a direct spin-resolved observation of the electronic band structure dynamics during optically induced demagnetization in a 3*d* ferromagnet.

## II. LIGHT SOURCES, PHOTOEMISSION SETUP AND SAMPLE PREPARATION

Our photoemission setup includes, in addition to our pulsed HHG source, an unpolarized, continuous wave (cw) He-discharge source emitting light at photon energies of $h\nu_I$ = 21.2 eV (He-I line) or $h\nu_{II}$ = 40.8 eV (He-II line). The light generated by the He lamp propagates in the vertical plane (that includes the detection direction) and illuminates the sample under an angle of 45° from above.

The femtosecond XUV pulses are generated by focusing <35 fs short laser pulses from a Ti:sapphire multipass laser amplifier system into a 50 mm long Ar-filled glass capillary[19] with an inner diameter of 150 $\mu$m. After the capillary, the generated XUV light propagates further in a vacuum environment to avoid absorption. The resulting spectrum has a comb-like structure consisting of odd harmonics of the driving laser.[7] The beam approaches the sample in the horizontal plane at an angle of 45° with respect to the detection direction (see Fig. 1(a)). The XUV light is linearly polarized and the polarization vector can be adjusted by the polarization of the fundamental laser.

In order to generate XUV pulses, we employ two modes: in the first mode the HHG source is driven by laser light of 1.59 eV with an energy per pulse of 2 mJ at a repetition rate of 3 kHz (referred to as "red-driven mode", RDM). In the second approach we use the frequency-doubled laser beam with 3.18 eV ("blue-driven mode", BDM). Here, the energy per pulse is 0.9 mJ or 0.6 mJ for a repetition rate of 3 kHz or 5 kHz, respectively. In the RDM, in general a light spectrum between 20 eV and 46 eV is available, which allows for the addressing of different parts of the BZ in $k_\perp$-direction.[25,26] To select the desired energy, we use one flat and one curved Si/Mo multilayer mirror placed under a small angle of incidence (5° with respect to the surface normal, see left side of Fig. 1(b)). The mirrors are designed to act as narrow-bandwidth Bragg monochromators selecting an energy window of ≈2 eV (FWHM) around a photon energy of $h\nu_{RDM}$ = 42.7 eV with a total transmission of ≈6 %. This arrangement ensures the selection of only one harmonic, a convenient focusing and a conservation of the temporal structure of the pulses.[18] The resulting XUV spectrum is shown as the red filled symbols in Fig. 1(c). Here, the energy-calibration has been done using the known separation of the neighboring harmonics and a comparison of sharp features in photoemission measurements with corresponding spectra acquired using the well-characterized He lamp. The light polarization was set to be horizontal for all presented results using the RDM.

The concept of the second mode of source operation, the BDM, is based on earlier observations showing a substantial increase in the conversion efficiency in a well-defined energy range by reducing the fundamental wavelength.[27,28] In combination with the low energy cutoff of a thin Al foil[29] at 20 eV, the BDM can be used to provide only a single pronounced harmonic[28] around $h\nu_{BDM}$ = 22.5 eV (blue open symbols in Fig. 1(c)). As a result, no monochromator is necessary and the XUV light is, after suppressing the fundamental laser light by a reflection from an oxidized Si wafer, focused on the sample using a toroidal Au mirror. Since both optical elements reflect the light at grazing incidence (85° with respect to the surface normal, see right side of Fig. 1(b)), the resulting total XUV reflectivity is higher than 70 % for vertically polarized light (calculated using "REFLEC"[30]). A vertical light polarization was adjusted for all presented measurements employing the BDM. We stress that the photon energies provided by our pulsed XUV source in RDM and BDM are very close to the He-I and the He-II lines of the gas-discharge lamp, respectively, and therefore allow a direct comparison of the photoemission results.

The light spectra in Fig. 1(c) also show that the neighboring harmonics are suppressed by more than one and two orders of magnitude in the RDM and the BDM, respectively. Remaining light from the fundamental laser beam is blocked by a 200 nm thick Al foil that has a transmission of ≈63 % at the XUV energies which are used.[29] In combination with differential pumping stages, this Al foil additionally separates the pressure in the Ar-filled volume of the HHG source and in the ultrahigh vacuum environment of the photoemission experiment, where a pressure in the range of $10^{-10}$ mbar is kept during the measurements.

The experimental chamber is housing sample fabrication and characterization devices as well as the photoelectron spectrometer and the spin detector. For the cleaning of substrates and the growth of the samples, the chamber is equipped with an ion sputtering source, a resistive heater, and an electron beam evaporator. During the experiments, the photoelectrons are first energy-filtered by a cylindrical sector analyzer. Then, they are further analyzed by a spin detector (Focus FERRUM) based on very low-energy electron scattering from an oxygen-passivated epitaxial Fe film.[23] In our setup, the spin detector is mounted so that it is sensitive to the vertical in-plane magnetization component of the sample.

To compensate for linear drifts of the photon flux during the experiment, we recorded the spin-resolved data by repeating the following measurement sequence: ($\tilde{I}_+$, $\tilde{I}_-$, $\tilde{I}_-$, $\tilde{I}_+$), where $\tilde{I}_\pm$ represents the electron counts measured for two opposite magnetization directions of the Fe film.[31] The spin

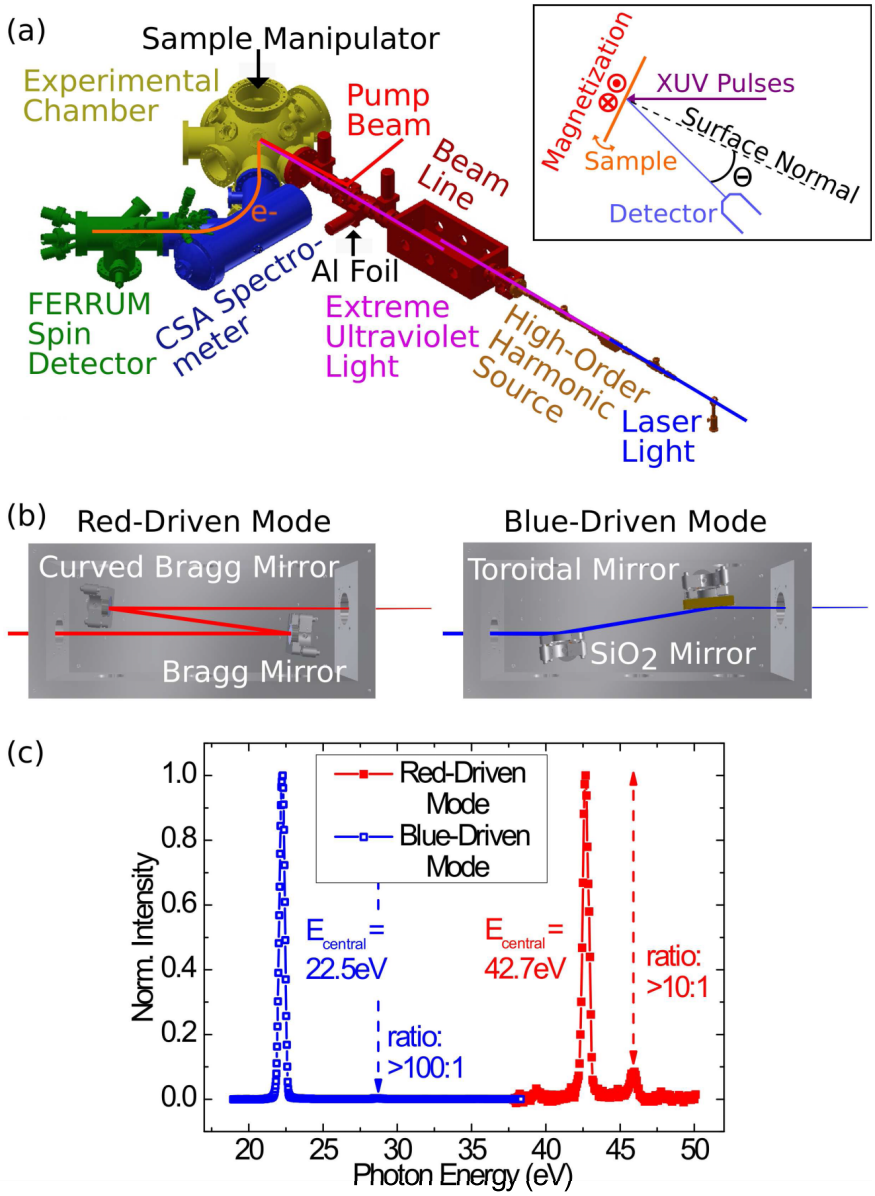


FIG. 1. (a) Experimental setup. The XUV radiation is guided through a beamline before it reaches the sample in the main chamber. Created photoelectrons are analyzed concerning their energy and their spin. The geometry at the sample is shown as the inset. (b) Monochromatizing and focusing optics in the beamline for the "red-driven mode" (left) and the "blue-driven mode" (right). (c) Light spectra resulting from both modes measured with an optical grating spectrometer.[24]

polarization $P$ is then given as

$$P = \frac{1}{S} \cdot \frac{I_+ - I_-}{I_+ + I_-}, \tag{1}$$

with the detector efficiency $S = 0.29$ (often referred to as Sherman function)[23] and $I_\pm$ being the summed up $\tilde{I}_\pm$ from several cycles. The relative intensity of each spin direction in the photoelectron beam $N_\pm$ (called partial intensity) can be calculated as

$$N_\pm = \frac{I_{tot}}{2}(1 \pm P), \tag{2}$$

with $I_{tot} = I_+ + I_-$. If not stated otherwise, the electron count rate is averaged in the energy range above $E_F$ in the raw data spectra and then the mean value between both spin directions is treated as an energy-independent background signal. This background is subtracted from the measured intensities before calculating the spin polarization and the partial intensities. The goal of the presented work is to test the suitability of our novel experimental setup for femtosecond time- and spin-resolved photoemission studies. To do that, we chose Co deposited on top of a Cu(001) crystal as a well-studied magnetic sample system.[32–34] The thin Co films were grown *in situ* by the following procedure: first, the Cu crystal was cleaned by Ar ion bombardment for 30 min at 1 kV and afterwards annealed for 10 min at 600 °C. Then, a Co layer of ≈30 ML was deposited at room temperature at a deposition rate of ≈1 ML/min. The deposition rate was estimated using the effective attenuation length (EAL) of the photoelectrons from 3*d* states of the Cu(001) crystal in the Co overlayer ($\lambda_{EAL} \approx 5.0$ ML at $h\nu = 24$ eV[35]). In order to avoid diffusion of Cu atoms into the Co films, no annealing was performed after deposition. The Co was magnetized along the vertical direction coinciding with the magnetic easy (110)

axis[36] and corresponding to the sensitive direction of the spin detector. All results presented below are measured in normal emission.

## III. SPIN-RESOLVED PHOTOELECTRON SPECTROSCOPY RESULTS

### A. Red-driven mode

In this subsection, we focus on our measurements performed with the XUV source in RDM ($h\nu_{RDM}$ = 42.7 eV)

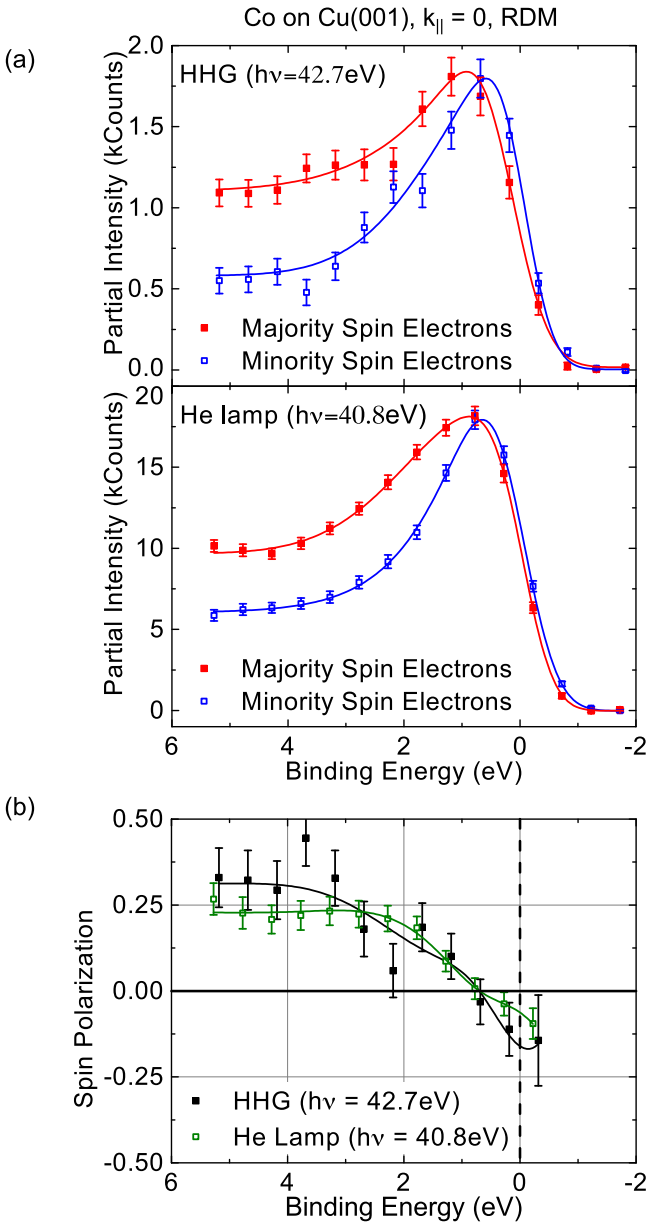


FIG. 2. (a) Partial intensities as a function of the binding energy. The squares represent data measured using the femtosecond-pulsed HHG source in "red-driven mode" (top) and the cw gas-discharge lamp (bottom). The spectrometer settings were identical for both cases and a sample bias of 16 V was applied in both measurements. Error bars are determined using the sum of the standard deviation of subsequent measurement cycles to account for fluctuations of the XUV source and $\sqrt{I_{\pm}}$ to consider the Poisson-characteristics of the count rate. The lines are calculated from fits to the measured spectra (see text). (b) Corresponding spin polarization distributions. Again, the lines are determined using the fits to the electron counts.

at a repetition rate of 3 kHz. The results are displayed in Fig. 2 together with data acquired using the He-II line of the cw gas-discharge lamp. Due to the similar photon energies of both light sources, the data can be directly compared to identify the influence of the pulsed excitation using the HHG source. For all measurements presented in Fig. 2, the spectrometer energy acceptance was set to a high value in order to increase the transmission of photoelectrons ($\Delta E_{Det}$ = 1.05 eV, see below). Furthermore, a positive sample bias was applied, which deflects additional electrons from higher emission angles into the spectrometer. Please note that the background subtraction routine for the measurement with the He-II line is slightly modified by first subtracting a background of spin-resolved photoelectrons, which are excited by satellite spectral lines.[37] The measured spectra ($I_{\pm}$) have been fitted with the convolution of a Gaussian peak function and the product of a Fermi-Dirac distribution ($T$ = 300 K) with another Gaussian peak function. Here, the first Gaussian function represents the combined energy resolution due to the spectrometer and the light source. The second Gaussian function takes into account the peak in the energy distribution curves (EDC). For the determination of the energy resolution of the experiment, we use the fit of the (raw data) intensity spectrum obtained in the measurement configuration that is mainly sensitive to minority spin electrons. The total chemical potential from this fit is used as the origin of the x-axis and the lines in Fig. 2 are calculated using the results of the fitting procedure.

The spectra show a broad cutoff at the Fermi edge that can be assigned to the energy resolution of the spectrometer $\Delta E_{Det}$. Because the spectral width of the He-II line is negligible, $\Delta E_{Det}$ can be determined from the broadening extracted from the fit of the He lamp measurement ($\Delta E_{He-II}$). Since $\Delta E_{Det} = \Delta E_{He-II} = 1.05 \pm 0.03$ eV has the same size as the broadening of the spectrum measured with the XUV pulses ($\Delta E_{RDM} = 1.00 \pm 0.10$ eV), the spectral width of the HHG source in RDM has within errors no influence on the energy resolution for the spectrometer settings used.

In general, $k_{\perp}$ is close to Γ in Co(001) for a photon energy of $h\nu$ = 42.7 eV. Band structure calculations predict[38] several different states in the vicinity of $k_{\perp} = 0$ including a minority spin state with $\Delta_{5\downarrow}$ and majority spin states with $\Delta_{1\uparrow}$ and $\Delta_{2\uparrow}$ character at $E_B$ = 0.8 eV. However, due to the spectrometer energy resolution used in the RDM measurements and the additionally applied sample bias, single band structure features cannot be resolved resulting in the EDCs with only a single, broad peak for each spin direction which are shown in Fig. 2(a). This also justifies the fitting of only one single Gaussian peak function to the spectra. For the spin polarization $P$ (see Fig. 2(b)), we find a constant value of ≈0.25 for high binding energies. At $E_B$ = 2.5 eV, $P$ starts to decrease and reaches zero at $E_B$ = 0.7 eV. Close to $E_F$, the spin polarization has a small negative value.

Comparing the measurements using the He-II line and the HHG source in RDM (see Fig. 2), only small deviations of the results, mostly visible in the spin polarisation distribution, are present. These differences can be mainly related to the statistical fluctuations due to the electron counts, which are limited for current laser systems and spin detectors (10 counts/s, >1700 counts total at the valence band maximum

for the presented measurement) within acquisition times suitable for pump-probe studies (<2 h for the presented data). Therefore, we note that the RDM is applicable for time-resolved studies only with restricted energy resolution and for specific electron energies and emission angles at the moment. However, we observed no fundamental restrictions for this mode of operation and the RDM will become increasingly important with improved laser systems due to the availability of a broad range of photon energies.

### B. Blue-driven mode

In the BDM, the higher XUV photon flux allows us to use detector settings with a four times better energy resolution, while still reaching more than one order of magnitude higher electron count rates of 400 counts/s and more than 9500 counts total at the valence band maximum.

In contrast to the results in RDM, the EDCs and thus the spin polarization measured with the pulsed XUV source (top of Fig. 3(a)) differ from those acquired with the He-I line (bottom). The main difference in the spectra is that the unpolarized light from the He lamp excites electrons from a Co surface resonance[39–41] resulting in an additional peak at $E_B = 0.62 \pm 0.07$ eV for the minority spin direction. Due to the even symmetry of this surface resonance,[39] the underlying transition is forbidden for the s-polarized light from the pulsed XUV source. The full suppression of the peak confirms the high degree of light polarization of our HHG source. Another remarkable point in the EDCs is the difference in the photoemission intensity for binding energies higher than 1 eV. Since both measurements were performed immediately one after the other, we exclude an influence of a surface contamination and attribute this observation to the light polarization as well, which allows additional excitations using the He lamp. The main peaks in the majority and minority spin channel can be assigned to an initial state with $\Delta_{2\uparrow}$ and $\Delta_{5\downarrow}$ character, respectively, by a comparison of our results with band structure calculations.[38,42,43] The disappearance of sharp features for higher binding energies can be attributed to the strong correlation effects in the studied sample system.[44–46]

In the measurements with the He-I line, a spin-polarized background is subtracted to account for the influence of the satellite spectral lines[37] before applying the standard background subtraction routine (similar to the measurements with the He-II line in Sec. III A). The measured intensities $I_\pm$ are fitted as in Sec. III A, but, in contrast to the single Gaussian function modeling the features in the EDCs in Fig. 3, this time two (three) Gaussian peaks are used for the HHG (He lamp) data. The additional terms take into account that the minority and majority spin electron peaks can be separated for the measurements in Fig. 3 and, in addition, that the surface resonance is observed in the results obtained with the He-I line. The energy resolution of the spectrometer can be again extracted from the fit of the minority spin dominated data acquired using the very narrow-bandwidth He lamp: $\Delta E_{Det} = \Delta E_{He-I} = 0.23 \pm 0.02$ eV. In the BDM measurement, where the detector energy resolution is also set to $\Delta E_{Det} = 0.23$ eV (instead of 1.05 eV in the RDM, see Sec. III A), the broadening of the spectra due to

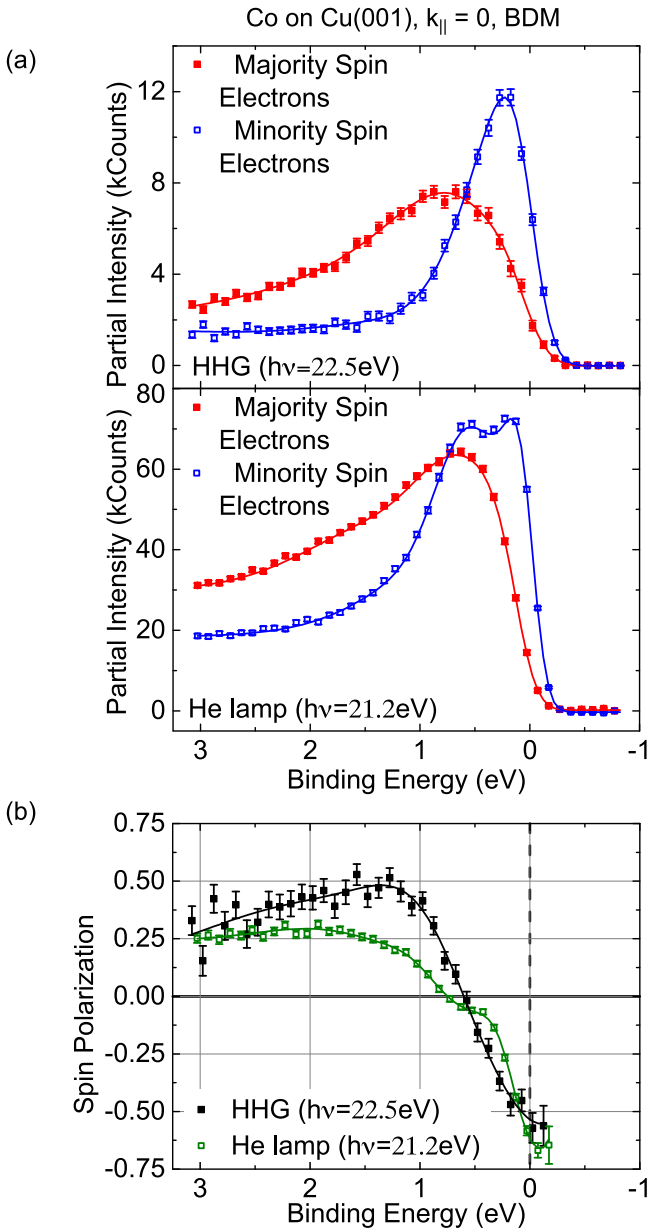


FIG. 3. (a) Energy distribution of the partial intensities for both spin directions. The data was taken with the HHG source in "blue-driven mode" (top) and the He-I line of the cw gas-discharge lamp (bottom) under the same conditions. The error bars are determined using the same procedure as in Fig. 2, and the lines are calculated from the fits to $I_\pm$. (b) Spin polarization for the spectra shown in (a).

the bandwidth of the HHG light is now observable ($\Delta E_{BDM} = 0.35 \pm 0.01$ eV). Assuming Gaussian distributions for the energy resolution of the spectrometer and the spectral width of the light source, the latter can be estimated as $\Delta h\nu_{BDM} = \sqrt{(\Delta E_{BDM})^2 - (\Delta E_{Det})^2} = 0.26 \pm 0.02$ eV. Please note that the spectral width of the femtosecond pulses is fundamentally limited by the time-bandwidth-product ($\Delta h\nu = 0.26$ eV at $h\nu = 22.5$ eV corresponds to band-width-limited pulses with a duration of $\Delta t = 7$ fs). Consequently, a further increase of the energy resolution has to be carefully adjusted to the required temporal resolution. A contribution from vacuum space-charge effects (see Sec. IV A) to the energetic broadening

was reduced by increasing the repetition rate of the pulsed XUV source to 5 kHz in the BDM and thus redistributing the photoelectrons to more pulses. In addition, the photon flux was reduced (see end of Sec. IV A).

In general, a direct comparison of our results measured with the He-I line and the HHG source in BDM is difficult due to the presence of the surface resonance. However, in the energy range where its influence is small ($E_B > 2$ eV and $E_B \approx 0$ eV), the spin polarization of both measurements is in good agreement. The count rates achieved in BDM allow the acquisition of spin-resolved spectra in less than 1 h, and therefore several EDCs can be measured with consistent sample conditions in an UHV environment. Consequently, our experiment using the HHG source in BDM is perfectly suited for femtosecond time- and spin-resolved PES.

## IV. VACUUM SPACE-CHARGE EFFECTS

### A. HHG-induced space-charge

As noted in Sec. III, vacuum space-charge effects play a significant role in photoemission experiments with ultrashort pulsed excitation. In this section, we will illustrate and quantify their influence for our PES experiments. This is necessary in order to determine an upper limit for the number of photoelectrons in our setup that still allows to measure without strong distortions. In contrast to cw light sources, the excitation with femtosecond pulses leads to the generation of quasi-two-dimensional disks of photoelectrons.[47] In order to achieve an electron count rate comparable with a cw source, a similar amount of photoelectrons has to be compressed into these disk-shaped clouds which results in a high electron density. As a consequence, the strong Coulomb-repulsion inside the electron clouds causes an energetic and angular distortion of spectral features depending on the photoelectron density. To illustrate the space-charge effects, Fig. 4(a) shows two normalized EDCs measured on Cu(001) employing the BDM with moderate (blue filled squares) and with more than 70 times higher intensity (black open circles) while all other parameters are the same. For the higher intensity, both a shift and a broadening of the peak created by the 3*d* electrons are clearly visible. This behavior has been already observed in photoemission measurements using pulsed light sources, e.g., with visible laser light,[47] FELs[48] and HHG sources.[49]

The processes causing the spectral distortions described above can be explained using the illustration in Fig. 4(b). Immediately after the creation of the electron cloud at the sample at the time $t_1$, each photoelectron experiences an individual acceleration or deceleration depending on the electron distribution in its near environment resulting in the observed energetic broadening.[50,51] During their propagation to the spectrometer entrance, the photoelectrons arrange according to their kinetic energies. In our measurements, we aim to detect the unscattered photoelectrons that originate

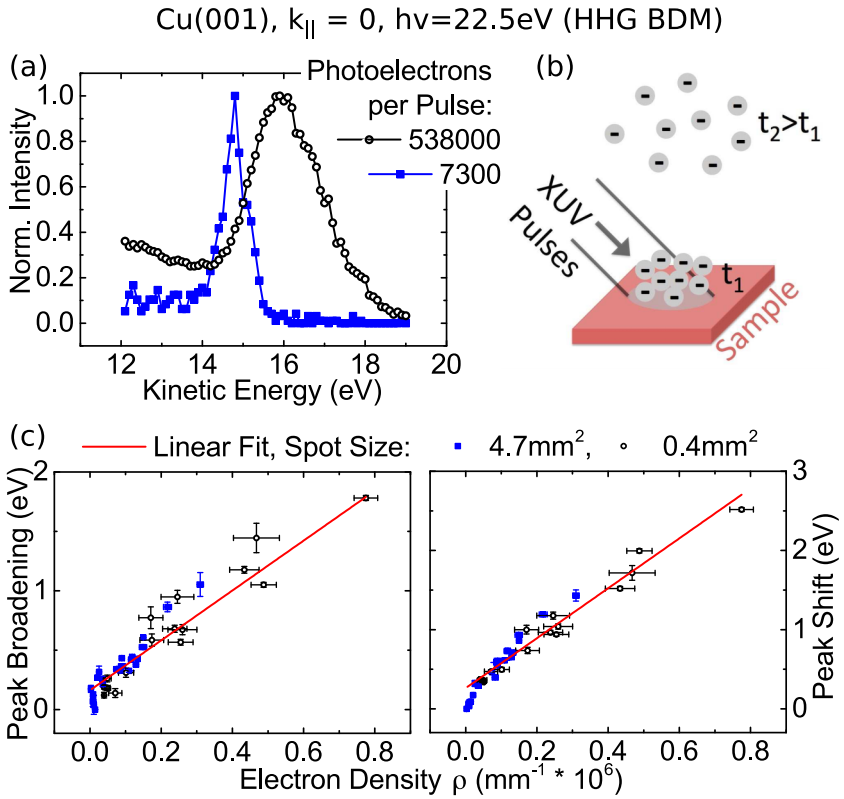


FIG. 4. (a) EDCs measured on the 3*d* peak ($E_{kin} = 14.5$ eV) of Cu(001) with different photon flux of the HHG source. (b) Schematic drawing of the evolution of dense electron clouds created by photoemission with ultrashort pulses (based on a drawing by Hellmann *et al.*[51]). (c) Broadening (left) and shift (right) of the Cu(001) 3*d* peak for two different sizes of the excitation area. The data is plotted as a function of the number of photoelectrons, normalized to the number of pulses and the diameter of the light spot. Values for $\rho > 0.025 \cdot 10^{-6}\,\mathrm{mm}^{-1}$ are fitted with a linear function (red line). The error bar determination is based on the standard deviation of the sample current for $\rho$ and on the uncertainties of the fit results for the peak shift and broadening.

from the valence bands. These electrons have a higher kinetic energy than the average energy of the electron cloud, which also contains the slow electrons that are caused by inelastic scattering events in the crystal. Therefore, the valence band electrons propagate at the front part of the cloud and are accelerated by the Coulomb repulsion of the following electrons on their way to the detector (see cloud shape at time $t_2$ in Fig. 4(b)). This effect leads to the shift of the peak towards higher kinetic energies.[50,51]

Since the energetic shift as well as the broadening depends on the photoelectron density, their influence can be further characterized by varying the photon flux and the size of the electron cloud. Here, the total number of photoelectrons was determined by a direct measurement of the photocurrent, while the peak width and position were extracted from the measured EDCs by fitting a Gaussian peak function. From the peak parameters, the shift was calculated by a linear subtraction of the minimum position and the broadening by the square root of the difference between the squared actual peak width and the squared minimum peak width. The initial diameter of the photoelectron disk was assumed to be equal to the spot diameter of the laser light driving the HHG process. We determined the latter from pictures of the sample surface taken with a CCD camera. The spot size can be adjusted by an iris aperture, which is placed between the $SiO_2$ and the toroidal mirror (see right side of Fig. 1(b)). This aperture also compensates the difference in the original divergence between the XUV beam and the fundamental laser light[52] to a large extend (see discussion at the end of this section).

The results for a spot size of $A_1 = 4.7\,\mathrm{mm}^2$ (blue filled squares) and $A_2 = 0.4\,\mathrm{mm}^2$ (black open circles) are plotted in Fig. 4(c). The plots show the broadening (left side of Fig. 4(c)) and the shift (right side of Fig. 4(c)) of the $3d$ electron peak of Cu(001) as a function of the number of photoelectrons per pulse $N$ normalized to the diameter of the spot $d$,

$$\rho = \frac{N}{d}. \tag{3}$$

The relation between the magnitude of the shift/broadening and the spot diameter leading to the definition of the linear photoelectron density $\rho$ as a function of $d^{-1}$ (in contrast to, e.g., a normalization to the spot area with $\rho_{area} \propto d^{-2}$) was found in earlier publications.[47,51] The dependence on $d^{-1}$ can be explained[51] because an electron in a two-dimensional disk of charges has a potential energy $\propto N/d$. This potential energy is then (partly) converted to kinetic energy resulting in the spectral changes. Our measurements are in agreement with this model since the broadening as well as the shift show the same dependence on $\rho \propto d^{-1}$ for $A_1$ and $A_2$.

Furthermore, the dependence on $\rho$, which is observed for both quantities if the number of photoelectrons is varied, is for high photoelectron densities compatible with existing numerical simulations for valence band spectroscopy.[51] The latter predict a linear behavior and also the higher slope for the peak shift than for the peak broadening. A fit of our data with the linear function $y = m \cdot x + b$ yields slopes of

$$m_{broadening} = 2.10 \cdot 10^{-6}\,\mathrm{eV\ mm} \tag{4}$$

and

$$m_{shift} = 3.15 \cdot 10^{-6}\,\mathrm{eV\ mm}. \tag{5}$$

Values for $\rho < 0.025 \cdot 10^{-6}\,\mathrm{mm}^{-1}$ are not considered in this analysis, because here the measured sample current approaches the background noise level. Furthermore, the values for the peak broadening and shift converge towards the intrinsic width of the Cu $3d$ peak (see Fig. 4(a)). The slopes that we extracted have twice the value of the numerical simulation results of Hellmann *et al.*, but deviations in this range have also been found by the authors in their publication in comparison with other experimental data.[51] Generally, a systematic error can in our case originate from the determination of the spot size using the fundamental laser and not the XUV light as discussed earlier. In order to estimate the resulting deviation, we performed raytracing simulations of our experimental situation (using the software "RAY"[53]), which result in approximately 20% smaller spots for the XUV radiation. This would then reduce the slopes $m_{broadening}$ and $m_{slope}$ to 80% of their original value.

Our measurements show that the peak broadening and shift caused by XUV-induced space-charge significantly exceed 1 eV for photoelectron densities that can be reached with our HHG source. However, the knowledge of $m_{broadening}$ and $m_{shift}$ allows us to tune the light intensity so that $\rho$ stays in a range, where the XUV-induced space-charge broadening discussed above is not significantly lowering the energy resolution of the experiment. For the measurements presented in Fig. 3 using the HHG source in BDM, the photon flux was reduced such that $\rho \approx 3.5 \cdot 10^4\,\mathrm{mm}^{-1}$ (spot size of driving laser: $A = 2.6\,\mathrm{mm}^2$). For the determined value of $m_{broadening}$ (see Eq. (4)), this corresponds to a space-charge broadening of $\Delta E_{sc} \approx 0.07$ eV. Extracting the resulting influence on $\Delta h\nu_{BDM}$ by a deconvolution yields a contribution of the space-charge broadening of less than 5% of the total value for the given conditions.

### B. Pump-induced space-charge

For the realization of time-resolved studies of the demagnetization dynamics in a pump-probe scheme, an additional laser beam for the triggering of the process has to be introduced. For this purpose, near-infrared (NIR) pump-pulses with fluences on the order of 1–10 $\mathrm{mJ/cm}^2$ per pulse are commonly used. It is well-known that such intense laser pulses, even though their photon energy is far below typical metallic work functions $\phi$ ($\phi_{Co} = 4.8$ eV for Co(001)[54]), create a significant electron background via non-linear photoemission. The energy distribution of the resulting photoelectrons has a tail reaching kinetic energies as high as the photoelectrons excited from the valence bands with our XUV beam.[55] The yield of this process strongly depends on the light peak intensity, light polarization, and the illuminated position of the sample surface. The latter fact points to a crucial role of the sample quality and surface roughness.[14,56,57] As the underlying physical process for the generation of these photoelectrons, usually thermally assisted multiphoton photoemission is considered[58–60] for the laser peak power range that we use. However, the mechanism for

the acceleration of the photoelectrons to high kinetic energies is still under debate.[56,57,61]

Since the NIR pump-induced photoelectrons also affect the XUV probe-induced electrons via Coulomb repulsion, they create an additional space-charge contribution which varies with the delay $\Delta t$ between pump- and probe-pulse. We investigated the interaction between the pump- and the probe-generated electron clouds using Cu(001) spectra measured for different $\Delta t$ with the femtosecond HHG source at 5 kHz in BDM. In the measurements, a pump fluence of $\approx 8\,\mathrm{mJ/cm^2}$ was applied which is a realistic value for magnetization dynamics measurements. It results in a ≈20 times higher photoelectron yield from the NIR than from the XUV beam. Please note that the number of NIR pump-induced photoelectrons and thus their influence can be substantially reduced without reducing the pump fluence, for example by a careful adjustment of the beam position as discussed above. However, in order to thoroughly characterize the additional space-charge contribution, we kept the number of NIR pump-induced photoelectrons high. For the separation of the Cu(001) spectra excited by the XUV light from the NIR pump-induced background, the data was collected by consecutive measurements with only the NIR beam and with both the XUV and the NIR beam illuminating the sample (see inset of Fig. 5(a)). Afterwards, we calculated the difference between both spectra. Figure 5(a) shows typical EDCs that result from this procedure (symbols) together with Gaussian peak function fits (lines) for selected delays. If the arrival time of the XUV probe-pulse is before the arrival time of the NIR pump-pulse ($\Delta t < 0$, red open triangles), the Cu 3*d* electron peak ($E_{kin}$ = 15 eV) is shifted towards higher kinetic energies compared to the situation without pump-beam (black filled triangles). The shift becomes more pronounced for smaller negative delays. Even for small positive delays (XUV probe-pulse after NIR pump-pulse, gray filled squares), the electrons are accelerated. On the other hand, at longer positive delays, the peak shows a shift to lower kinetic energies (green open squares).

The full dependence of the peak shift on the delay $\Delta t$ is shown by the black squares on the left side of Fig. 5(b). Delay ranges, which are represented by the spectra shown in Fig. 5(a), are shaded in the corresponding color. If the XUV

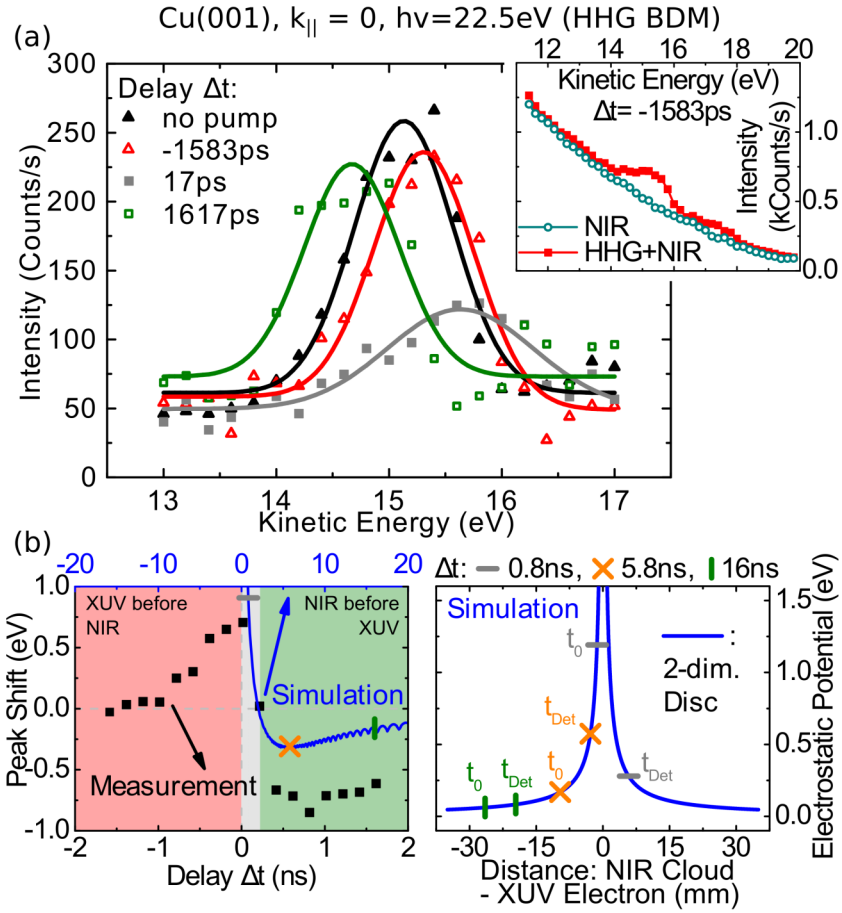


FIG. 5. (a) EDCs of the 3*d* electron peak after background subtraction for varying delays between the pump- and probe-pulses. The lines represent Gaussian peak function fits. Inset: Photoemission intensity as a function of the electron kinetic energy for Cu(001). The green open circles illustrate the photoelectron background generated only by the pump-pulse. For the measurement represented by the red filled squares, the near-infrared as well as the XUV pulses contribute to the excitation. (b) Left: Delay-dependence of the peak shift caused by vacuum space-charge effects from the pump-induced electrons. The black squares represent the measurement results extracted from Gaussian peak function fits as shown in (a). The blue curve is the result of a simulation yielding the final kinetic energy of a probe electron at the detector entrance for each delay. In the simulation, the trajectory of this probe electron in the electrostatic potential of a moving electron cloud is calculated (see text). The oscillations in the curve are caused by the discretization of the energy distribution of the pump-induced photoelectrons. Right: Electrostatic potential of a two-dimensional electron disk plotted against the distance to this disk. The markers highlight the potential energy of the probe electron at the sample and the spectrometer distance for characteristic situations, which are also indicated in the plot on the left side.

probe-pulse arrives at the sample before the NIR pump-pulse ($\Delta t < 0$), we always observe a positive shift of the Cu(001) 3*d* peak with an amplitude that increases towards $\Delta t = 0$. This behavior is similar to results from FEL measurements reported by Oloff *et al.*[62] Here, the authors argue that the NIR pump-induced electrons are created after the excitation of the electrons from the valence band by the FEL probe-pulses. Since most of the mainly "slow" NIR pump-induced electrons stay behind the faster valence band electrons, the latter always experience an accelerating repulsion.

In contrast, the sharp drop in the peak shift followed by *negative values* for $\Delta t > 0$ observed in our measurements has, to our knowledge, not been explained so far. We interpret this behavior in the way that the XUV probe-induced electrons are not fast enough to overtake the majority of the NIR pump-induced electron cloud before they reach the spectrometer entrance for the corresponding delays. Therefore, the XUV probe-induced electrons travel most of the way behind the pump-induced electron cloud and are decelerated. This is in contrast to the experimental situation of Oloff *et al.*, where the probe-induced electrons are significantly faster ($E_{kin} \approx 3000$ eV) than the NIR pump-induced electrons.

For a better understanding, we performed simulations for our situation. Here, the NIR pump-generated electron cloud (in the following called "NIR cloud") is modeled by several charged disks moving with different kinetic energies which in total represent a typical pump-induced photoelectron spectrum. Internal interactions are neglected. By subsequently calculating the velocity of a single probe electron (in the following called "XUV electron") for increasing times in the changing electrostatic potential of the NIR cloud,[63] the final kinetic energy of the XUV electron after propagating the distance between sample and detector can be determined. The resulting energy shift compared to an undisturbed electron is shown as the blue curve on the left side of Fig. 5(b) for conditions representing our experimental situation. Please note that the time scale of the plots for the measurement and calculation results differ by a factor of 10. Possible reasons for this difference are discussed at the end of this section.

In order to illustrate the basic idea and the findings of the model, the right side of Fig. 5(b) shows the potential energy of the XUV electron at its emission (time $t_0$) and after propagating the distance to the detector (time $t_{Det}$) in the field of a moving, two-dimensional electron disk for three characteristic delays. The relative positions are taken from the simulation and represent the distance between the XUV electron and the part of the NIR cloud propagating with a kinetic energy equal to the weighted mean of the entire cloud. A difference in the potential energy at $t_0$ and $t_{Det}$ leads to a shift of the kinetic energy.

For small positive delays ($\Delta t = 0.8$ ns, gray horizontal lines), the XUV electron is emitted after the NIR cloud, but when the latter is still close to the sample leading to a high potential energy at $t_0$. Then, the XUV electron, which originates from the valence bands and has therefore a high kinetic energy, overtakes the NIR cloud and reaches the detector "long" before the NIR cloud ($t_{Det}$). The XUV electron has thus almost no potential energy left resulting in an acceleration. For higher delays, the distance of the NIR cloud at the time of emission of the XUV electron increases resulting in a decrease of the potential energy of the XUV electron at $t_0$. In parallel, the XUV electron reaches the detector while being strongly influenced by the NIR cloud. At a certain point, the potential energy at $t_{Det}$ exceeds the value at $t_0$ and the XUV electron is decelerated ($\Delta t = 5.8$ ns, orange crosses). If the delay is further increased ($\Delta t = 16$ ns, green vertical lines), the potential energy at $t_{Det}$ is lower again and the situation approaches the undisturbed case, where the XUV electron stays far behind the NIR cloud.

Our model can qualitatively reproduce the behavior that we observe in the experiment including the negative shifts. However, for a better quantitative agreement of the size of the energy shifts as well as the time scales, additional effects have to be included into our model in future. This includes mirror charges in the sample created by the pump-induced photoelectrons, which reduce the potential. In addition, the NIR cloud was modeled by a Gaussian distribution ($E_{central} = 5$ eV, FWHM $\approx$16.5 eV) but its shape can significantly vary depending on the exact experimental situation. Several other effects, e.g., repulsion within the NIR cloud, the influence of other electrons, and the inner structure of the electron clouds, have been neglected in the model for simplicity reasons. Furthermore, the trajectories in the calculations are limited to the normal emission direction and interactions happening after the electrons enter the spectrometer are not taken into account. More sophisticated simulations including the effects mentioned above may be able to fully reproduce the observed delay-dependence.

## V. CONCLUSION AND POTENTIAL FOR ULTRAFAST MAGNETIZATION DYNAMICS MEASUREMENTS

The main motivation for our work is to test our novel femtosecond time- and spin-resolved photoelectron spectroscopy setup. The experiment is intended for measurements of the electron and spin dynamics in the band structure of 3*d* ferromagnets.

Our results show the potential of the RDM that provides a broad range of photon energies. This mode will become more relevant with improving HHG sources and spin detectors that allow to overcome the limitation of electron count rates in spin-resolved measurements.

In the BDM, our setup allows spin-resolved acquisition times below 1 h at an energy resolution better than 0.4 eV. This is well-suited for pump-probe studies of magnetism in 3*d* ferromagnets. The energy resolution can be tuned by adjusting the spectral width of the XUV pulses to the needed temporal resolution, e.g., by further optimizations of the HHG source[28,64] or the use of grating monochromators.[20] Moreover, our results show that the electron count rate is mainly limited by vacuum space-charge effects in the BDM. Recent developments already address this problem by optimizing the HHG sources for high-repetition rate photoemission experiments.[65,66]

In view of time-resolved studies, we characterized the influence of photoelectrons created by NIR pump-pulses with variable arrival time. We observed that the NIR

pump-generated electrons can introduce significant energy shifts of the spectra. Therefore, the pump-induced photoelectron background has to be minimized by, e.g., minimizing the sample surface roughness or by stretching the pump-pulse duration. In addition, we were able to qualitatively explain the observed behavior including the negative shifts of spectral features. Our results show that the influence of the pump-induced electron cloud on the XUV-induced photoemission spectra via space-charge is varying on a time scale of several tens of pico- to nanoseconds. Therefore, the peak position can be assumed as constant within the time window relevant for studies of laser-induced demagnetization dynamics, which takes place within less than 1 ps after $\Delta t = 0$. The data point located at $\Delta t = +17$ ps, which still represents a shift to positive values comparable to the situation at $\Delta t \leq 0$, confirms this finding.

The presented results confirm the potential of our experimental approach using a state-of-the-art spin detector based on exchange scattering and a modern, laser-driven HHG light source for studies of ultrafast band structure dynamics in ferromagnetic materials with spin- and energy-resolved photoemission.

## ACKNOWLEDGMENTS

This work was supported by the Deutsche Forschungsgemeinschaft through Nos. SCHN 353/17-1 and AE 19/20-1 (Element-spezifische Untersuchung von Femtosekunden Magnetisierungsdynamik). We would like to thank L.-P. Oloff and K. Rossnagel for helpful discussions about vacuum space-charge effects and B. Küpper and J. Lauer for technical support.

[1]E. Beaurepaire, J.-C. Merle, A. Daunois, and J.-Y. Bigot, Phys. Rev. Lett. **76**, 4250 (1996).
[2]B. Koopmans, G. Malinowski, F. Dalla Longa, D. Steiauf, M. Fähnle, T. Roth, M. Cinchetti, and M. Aeschlimann, Nat. Mater. **9**, 259 (2010).
[3]M. Battiato, K. Carva, and P. M. Oppeneer, Phys. Rev. Lett. **105**, 027203 (2010).
[4]J. Hohlfeld, E. Matthias, R. Knorren, and K. H. Bennemann, Phys. Rev. Lett. **78**, 4861 (1997).
[5]K. Tiedtke, A. Azima, N. Von Bargen, L. Bittner, S. Bonfigt, S. Düsterer, B. Faatz, U. Frühling, M. Gensch, C. Gerth *et al.*, New J. Phys. **11**, 023029 (2009).
[6]R. W. Schoenlein, S. Chattopadhyay, H. H. W. Chong, T. E. Glover, P. A. Heimann, W. P. Leemans, C. V. Shank, A. Zholents, and M. Zolotorev, Appl. Phys. B **71**, 1 (2000).
[7]T. Pfeifer, C. Spielmann, and G. Gerber, Rep. Prog. Phys. **69**, 443 (2006).
[8]C. Stamm, T. Kachel, N. Pontius, R. Mitzner, T. Quast, K. Holldack, S. Khan, C. Lupulescu, E. F. Aziz, M. Wietstruk *et al.*, Nat. Mater. **6**, 740 (2007).
[9]B. Pfau, S. Schaffert, L. Müller, C. Gutt, A. Al-Shemmary, F. Büttner, R. Delaunay, S. Düsterer, S. Flewett, R. Frömter *et al.*, Nat. Commun. **3**, 1100 (2012).
[10]D. Rudolf, C. La-O-Vorakiat, M. Battiato, R. Adam, J. M. Shaw, E. Turgut, P. Maldonado, S. Mathias, P. Grychtol, H. T. Nembach *et al.*, Nat. Commun. **3**, 1037 (2012).
[11]S. Mathias, J. M. Shaw, E. Turgut, P. Grychtol, R. Adam, D. Rudolf, H. T. Nembach, T. J. Silva, M. Aeschlimann, C. M. Schneider *et al.*, J. Electron Spectrosc. Relat. Phenom. **189**, 164 (2013).
[12]A. Scholl, L. Baumgarten, R. Jacquemin, and W. Eberhardt, Phys. Rev. Lett. **79**, 5146 (1997).
[13]B. Heitkamp, F. Kronast, L. Heyne, H. A. Dürr, W. Eberhardt, S. Landis, and B. Rodmacq, J. Phys. D: Appl. Phys. **41**, 164002 (2008).
[14]H.-S. Rhie, H. A. Dürr, and W. Eberhardt, Phys. Rev. Lett. **90**, 247201 (2003).
[15]A. Weber, F. Pressacco, S. Günther, E. Mancini, P. M. Oppeneer, and C. H. Back, Phys. Rev. B **84**, 132412 (2011).
[16]S. Hellmann, M. Beye, C. Sohrt, T. Rohwer, F. Sorgenfrei, H. Redlin, M. Kalläne, M. Marczynski-Bühlow, F. Hennies, M. Bauer *et al.*, Phys. Rev. Lett. **105**, 187401 (2010).
[17]R. Haight, J. Bokor, J. Stark, R. H. Storz, R. R. Freeman, and P. H. Bucksbaum, Phys. Rev. Lett. **54**, 1302 (1985).
[18]S. Mathias, L. Miaja-Avila, M. M. Murnane, H. C. Kapteyn, M. Aeschlimann, and M. Bauer, Rev. Sci. Instrum. **78**, 083105 (2007).
[19]T. Rohwer, S. Hellmann, M. Wiesenmayer, C. Sohrt, A. Stange, B. Slomski, A. Carr, Y. Liu, L. Avila, M. Kalläne *et al.*, Nature **471**, 490 (2011).
[20]R. Carley, K. Döbrich, B. Frietsch, C. Gahl, M. Teichmann, O. Schwarzkopf, P. Wernet, and M. Weinelt, Phys. Rev. Lett. **109**, 057401 (2012).
[21]I. Gierz, J. C. Petersen, M. Mitrano, C. Cacho, I. C. E. Turcu, E. Springate, A. Stöhr, A. Köhler, U. Starke, and A. Cavalleri, Nat. Mater. **12**, 1119 (2013).
[22]A. Fognini, T. U. Michlmayr, G. Salvatella, C. Wetli, U. Ramsperger, T. Bähler, F. Sorgenfrei, M. Beye, A. Eschenlohr, N. Pontius *et al.*, Appl. Phys. Lett. **104**, 032402 (2014).
[23]M. Escher, N. B. Weber, M. Merkel, L. Plucinski, and C. M. Schneider, e-J. Surf. Sci. Nanotechnol. **9**, 340 (2011).
[24]C. La-O-Vorakiat, M. Siemens, M. M. Murnane, H. C. Kapteyn, S. Mathias, M. Aeschlimann, P. Grychtol, R. Adam, C. M. Schneider, J. M. Shaw *et al.*, Phys. Rev. Lett. **103**, 257402 (2009).
[25]C. M. Schneider, J. J. de Miguel, P. Bressler, P. Schuster, R. Miranda, and J. Kirschner, J. Electron Spectrosc. Relat. Phenom. **51**, 263 (1990).
[26]C. M. Schneider, C. Wiemann, M. Patt, V. Feyer, L. Plucinski, I. P. Krug, M. Escher, N. Weber, M. Merkel, O. Renault *et al.*, J. Electron Spectrosc. Relat. Phenom. **185**, 330 (2012).
[27]E. L. Falcão-Filho, C.-J. Lai, K.-H. Hong, V.-M. Gkortsas, S.-W. Huang, L.-J. Chen, and F. X. Kärtner, Appl. Phys. Lett. **97**, 061107 (2010).
[28]S. Eich, A. Stange, A. V. Carr, J. Urbancic, T. Popmintchev, M. Wiesenmayer, K. Jansen, A. Ruffing, S. Jakobs, T. Rohwer *et al.*, J. Electron Spectrosc. Relat. Phenom. **195**, 231 (2014).
[29]B. L. Henke, E. M. Gullikson, and J. C. Davis, At. Data Nucl. Data Tables **54**, 181 (1993).
[30]F. Schäfers, *Technischer Bericht: Berliner Elektronenspeicherring-Gesellschaft für Synchrotronstrahlung* (BESSY, 1996).
[31]A. Winkelmann, D. Hartung, H. Engelhard, C.-T. Chiang, and J. Kirschner, Rev. Sci. Instrum. **79**, 083303 (2008).
[32]J. J. De Miguel, A. Cebollada, J. M. Gallego, R. Miranda, C. M. Schneider, P. Schuster, and J. Kirschner, J. Magn. Magn. Mater. **93**, 1 (1991).
[33]A. K. Schmid and J. Kirschner, Ultramicroscopy **42**, 483 (1992).
[34]G. J. Mankey, R. F. Willis, and F. J. Himpsel, Phys. Rev. B **48**, 10284 (1993).
[35]C. M. Schneider, "Electronic structure and magnetic properties of ultrathin epitaxial films: fcc-Cobalt on Cu(100)," Ph.D. thesis, Freie Universität Berlin, 1990.
[36]P. Krams, F. Lauks, R. Stamps, B. Hillebrands, and G. Güntherodt, Phys. Rev. Lett. **69**, 3674 (1992).
[37]G. Schonhense and U. Heinzmann, J. Phys. E: Sci. Instrum. **16**, 74 (1983).
[38]C.-T. Chiang, A. Winkelmann, P. Yu, J. Kirschner, and J. Henk, Phys. Rev. B **81**, 115130 (2010).
[39]K. Miyamoto, K. Iori, K. Sakamoto, H. Narita, A. Kimura, M. Taniguchi, S. Qiao, K. Hasegawa, K. Shimada, H. Namatame *et al.*, New J. Phys. **10**, 125032 (2008).
[40]A. B. Schmidt, M. Pickel, T. Allmers, M. Budke, J. Braun, M. Weinelt, and M. Donath, J. Phys. D: Appl. Phys. **41**, 164003 (2008).
[41]L. Plucinski, A. Oelsner, F. Matthes, and C. M. Schneider, J. Electron Spectrosc. Relat. Phenom. **181**, 215 (2010).
[42]K. Miyamoto, K. Iori, K. Sakamoto, A. Kimura, S. Qiao, K. Shimada, H. Namatame, and M. Taniguchi, J. Phys.: Condens. Matter **20**, 225001 (2008).
[43]C. M. Schneider, P. Schuster, M. Hammond, H. Ebert, J. Noffke, and J. Kirschner, J. Phys.: Condens. Matter **3**, 4349 (1991).
[44]M. Ellguth, "A spin- and momentum-resolved photoemission study of strong electron correlation in Co/Cu(001)," Ph.D. thesis, Martin-Luther-Universität Halle-Wittenberg, 2015.
[45]S. Monastra, F. Manghi, C. A. Rozzi, C. Arcangeli, E. Wetli, H.-J. Neff, T. Greber, and J. Osterwalder, Phys. Rev. Lett. **88**, 236402 (2002).
[46]A. Grechnev, I. Di Marco, M. I. Katsnelson, A. I. Lichtenstein, J. Wills, and O. Eriksson, Phys. Rev. B **76**, 035107 (2007).
[47]S. Passlack, S. Mathias, O. Andreyev, D. Mittnacht, M. Aeschlimann, and M. Bauer, J. Appl. Phys. **100**, 024912 (2006).
[48]A. Pietzsch, A. Föhlisch, M. Beye, M. Deppe, F. Hennies, M. Nagasono, E. Suljoti, W. Wurth, C. Gahl, K. Döbrich *et al.*, New J. Phys. **10**, 033004 (2008).

[49]B. Frietsch, R. Carley, K. Döbrich, C. Gahl, M. Teichmann, O. Schwarzkopf, P. Wernet, and M. Weinelt, Rev. Sci. Instrum. **84**, 075106 (2013).
[50]X. J. Zhou, B. Wannberg, W. L. Yang, V. Brouet, Z. Sun, J. F. Douglas, D. Dessau, Z. Hussain, and Z.-X. Shen, J. Electron Spectrosc. Relat. Phenom. **142**, 27 (2005).
[51]S. Hellmann, K. Rossnagel, M. Marczynski-Bühlow, and L. Kipp, Phys. Rev. B **79**, 035402 (2009).
[52]J. Peatross and D. D. Meyerhofer, Phys. Rev. A **51**, R906 (1995).
[53]F. Schäfers, *Modern Developments in X-Ray and Neutron Optics* (Springer, 2008), pp. 9–41.
[54]W. Wallauer and T. Fauster, Phys. Rev. B **54**, 5086 (1996).
[55]D. M. Riffe, R. M. More, X. Y. Wang, M. C. Downer, D. L. Fisher, T. Tajima, and J. L. Erskine, JOSA B **10**, 1424 (1993).
[56]M. Aeschlimann, C. A. Schmuttenmaer, H. E. Elsayed-Ali, R. J. D. Miller, J. Cao, Y. Gao, and D. A. Mantell, J. Chem. Phys. **102**, 8606 (1995).
[57]G. Banfi, G. Ferrini, M. Peloi, and F. Parmigiani, Phys. Rev. B **67**, 035428 (2003).
[58]R. Yen, J. Liu, and N. Bloembergen, Opt. Commun. **35**, 277 (1980).
[59]G. Ferrini, F. Banfi, C. Giannetti, and F. Parmigiani, Nucl. Instrum. Methods Phys. Res., Sect. A **601**, 123 (2009).
[60]S. Hellmann, C. Sohrt, M. Beye, T. Rohwer, F. Sorgenfrei, M. Marczynski-Bühlow, M. Kalläne, H. Redlin, F. Hennies, M. Bauer *et al.*, New J. Phys. **14**, 013062 (2012).
[61]J. Kupersztych, P. Monchicourt, and M. Raynaud, Phys. Rev. Lett. **86**, 5180 (2001).
[62]L. P. Oloff, M. Oura, K. Rossnagel, A. Chainani, M. Matsunami, R. Eguchi, T. Kiss, Y. Nakatani, T. Yamaguchi, J. Miyawaki *et al.*, New J. Phys. **16**, 123045 (2014).
[63]B. J. Siwick, J. R. Dwyer, R. E. Jordan, and R. J. D. Miller, J. Appl. Phys. **92**, 1643 (2002).
[64]H. Wang, Y. Xu, S. Ulonska, P. Ranitovic, J. S. Robinson, and R. A. Kaindl, Nat. Commun. **6**, 7459 (2015).
[65]C.-T. Chiang, A. Blättermann, M. Huth, J. Kirschner, and W. Widdra, Appl. Phys. Lett. **101**, 071116 (2012).
[66]S. Hädrich, A. Klenke, J. Rothhardt, M. l. Krebs, A. Hoffmann, O. Pronin, V. Pervak, J. Limpert, and A. Tünnermann, Nat. Photonics **8**, 779 (2014).